UNCLASSIFIED

AAEC/E123

AUSTRALIAN ATOMIC ENERGY COMMISSION

RESEARCH ESTABLISHMENT

LUCAS HEIGHTS

BUCKLING AND INTEGRAL SPECTRUM MEASUREMENTS IN U235/BeO SUB-CRITICAL ASSEMBLIES

by

P. DUERDEN

D. B. McCULLOCH *

E. BRITTLIFF

* On attachment to A.A.E.C., Lucas Heights, from U.K.A.E.A., Reactor Group

Issued Sydney, July 1964

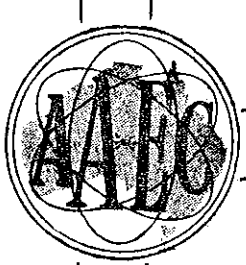

UNCLASSIFIED

AUSTRALIAN ATOMIC ENERGY COMMISSION

RESEARCH ESTABLISHMENT

LUCAS HEIGHTS

BUCKLING AND INTEGRAL SPECTRUM MEASUREMENTS IN U235/BeO SUB-CRITICAL ASSEMBLIES

by

P. DUERDEN

D. B. McCULLOCH *

E. BRITTLIFF

ABSTRACT

The materials buckling of four BeO moderated U235/aluminium alloy fuelled systems having BeO/U235 ratios of 1465, 2930, 5860, and 8790 have been measured by the exponential method. Relative fission rates of U235, U233, and Pu239 were also measured in the equilibrium spectrum region of the same assemblies. The experiments are described in detail, and the results compared with the predictions of a simple spectrum model (Westcott) pending analysis using more complex calculational models.

* On attachment to A.A.E.C., Lucas Heights, from U.K.A.E.A., Reactor Group.

CONTENTS

(continued)

CONTENTS (continued)

1. INTRODUCTION

The A.A.E.C.'s feasibility study of a BeO moderated high temperature gas-cooled reactor system requires survey calculations using computer codes capable of dealing in detailed manner with the neutron energy spectrum throughout the range from fission to thermal energies. Codes of this type (GMAC, SKATE, and MULGA) have been developed for this purpose at Lucas Heights.

Experimental data on beryllium-moderated systems, against which these codes and the adequacy of the nuclear data used herewith may be checked, have to date been restricted to measurements of the materials buckling or reactivity in a number of U235 fuelled systems (for example Kloverstrom et al. (1959) and (1960), Kloverstrom and Kraft (1960), Morton et al. (1962), Finke (1962)). The present series of experiments was carried out to augment the existing data by providing integral spectrum measurements to test the adequacy of the spectrum calculations, and to check the techniques of buckling measurement as a preliminary to proposed future experiments incorporating resonance absorbers (U238, Th232).

2. MATERIALS

The beryllium oxide and measurement of its diffusion properties for thermal neutrons, have been described by Brittliff et al. (1963).

The U235/aluminium alloy contained 23.4 $^{w}/_{o}$ of uranium enriched to 89.41V in the 235 isotope, and was in the form of strips, 24 in. long by 1.330 in. wide by 0.040 in. thick, each containing approximately 14.5g of U235. A total of 144 strips was available and used for these experiments.

Lattice plates to retain the fuel strips in the required configuration were made by milling slots 1.4" wide by 0.050" deep on a 2" pitch in 0.080" thick 99.95 per cent. pure aluminium sheets. Sheets 24" x 18" and 24" x 6" were available, thus enabling stack widths of either 18" or 24" to be obtained. Details of the alloy strips and lattice plates are given in Appendix V.

3. EXPERIMENTAL ARRANGEMENTS

The four lattices in which measurements were made were chosen to give BeO/U235 atomic ratios of:

I	1460
II	2930
III	5860
IV	8790

For Lattices I and II, the stack was approximately 18" x 18.3" x 24" high; for Lattices III and IV, the stack was approximately 24" x 25" x 24" high. The fuel strips were in all cases orientated with long dimension vertical, that is, perpendicular to the source plane. A typical section of each lattice is shown in Figures 1 to 4, and the composition of each is detailed in Appendix V.

A 16" high graphite plinth of slightly larger dimensions (1" each way) than those of the stack to be built, was placed centrally over the IR-1 stringer hole of the Argonaut-type reactor MOATA (Marks 1962). This plinth was supported approximately ¼" clear of the concrete top face of the reactor shield by 2" wide x ¼" thick strips of steel under two of its extreme edges. This made it possible to slide a cadmium sheet beneath the assembly for 'background flux' measurements without having to dismantle the stack. The plinth was surrounded by cadmium sheet and lead bricks to reduce the thermal neutron and γ-radiation in the vicinity to acceptable levels.

The BeO stack with the required lattice plates was constructed centrally on the graphite plinth. The top and sides of the stack were then clad with cadmium sheets. In addition, aluminium sheets were placed in contact with the cadmium cladding of the stack sides, and the whole assembly was clamped firmly together by means of a light aluminium angle frame retained in position by external threaded steel tie-rods. A general view of a completed stack before addition of the top cadmium sheet is shown in Figure 5. Diagrams of the two stacks used, showing positions of horizontal and vertical flux scanning holes, are given in Figures 6 and 7.

The entire experimental area surrounding the stack was enclosed in a polythene "tent", constructed on a light Dexion framework. The tent was fitted with filtered air extract equipment, and effectively checked any spread of beryllia contamination within the building. There was no neutron-reflecting material within 3 feet of the free boundaries of the stack, and even at these distances, the quantities were insignificant. All significant reflectors (building structure) were at least 20 feet from the sides and top of the stacks.

4. MEASUREMENT OF THE MATERIALS BUCKLING

Measurements were made of the vertical and horizontal flux distributions in the stack using ¼" diameter BF_3 proportional counters (20th Century Electronics Ltd. - Type 5EB/6). Except for measurements on Lattice I for which mains-frequency controlled time intervals were used, each count was made with reference to a pre-determined number of pulses from a 1" diameter BF_3 chamber positioned in the reactor shield tank water. In this way, the effects of drifts in reactor power were eliminated. Furthermore, the counter was frequently returned to a fixed "monitor" position in the stack as a check on drift in sensitivity of the counters and their associated electronic equipment.

4.1 Extrapolated Widths

Horizontal scans were made at two different heights in each stack (~12" and ~18" above the top face of the plinth) in both x and y directions. Measurements were also made with the counter covered by cadmium to ensure that only measurements made in the region of equilibrium spectrum were included in the subsequent analysis.

4.2 Relaxation Lengths

Vertical scans were made in at least two positions, one close to the centre of the stack, and the others at positions about one-third of the distance between the stack centre and a corner. Cadmium ratio measurements were again made as for the horizontal scans. In addition, further vertical scans were made with two sheets of 0.030" thick cadmium placed between the IR-1 hole and the reactor plinth. By subtraction, it was then possible to obtain the vertical flux distribution due to the required source below the stack alone, unperturbed by contributions from any in-leakage of fast neutrons through the sides and top of the assembly, or to γ-n neutrons produced by direct gamma radiation from the reactor core.

4.3 Errors

The following sources of error were considered in assessing the error on the flux measurements at each position in the stack. The magnitude of each source is given as its contribution to the error of the measured flux.

(a) Counting Statistics: Not less than 40,000 counts were accumulated at each position, giving a maximum error contribution of ±½ per cent.

(b) Control Channel Statistics: The control channel counts were never less than 400,000 whilst accumulating the data at any position. The control channel statistical error therefore contributed always less than ±0.16 per cent.

(c) Counter Positioning: The accuracy of location was approximately $\pm\frac{1}{32}$". The counter was independently located not less than twice in obtaining the flux at each position. The corresponding contribution to the error varies from lattice to lattice up to a maximum of ±0.35 per cent.

(d) Paralysis Time: The maximum correction for paralysis-time counting losses was 0.4 per cent. The paralysis time was known to within ±25 per cent., giving a maximum error contribution of ±0.1 per cent.

(e) Counter Drift: Checks carried out in fixed positions over extended periods, suggested that the error due to relative drifts in sensitivity between the experimental and control channel was about ±0.3 per cent.

(f) Background Measurements: In relaxation length measurements, the background to be subtracted was approximately 40 per cent. of the total flux, and was measured to better than ± 1 per cent.

The above sources of error are independent, and combine quadratically to give errors of 0.5 – 0.7 per cent. for horizontal scan fluxes, and 0.7 – 1.2 per cent. for vertical scan fluxes.

4.4 Results

The measured flux distributions for each lattice are given in Appendices I to IV.

4.4.1 E–W Widths (X–widths)

Flux measurements were made at 1″ intervals to within approximately 4″ of the stack edges. This region was confirmed to be of adequately constant spectrum by subsequent cadmium ratio measurements.

Owing to the heterogeneity of the lattices, it was necessary in all cases except Lattice II, for which analysis was straightforward, to make fine–structure corrections to the measured horizontal flux scans before fitting the data to cosine distributions. This was done as follows:

Lattice I. A set of measurements taken at 1″ intervals was split into two interleaved sets of 2″ interval scans. Each set was then composed of fluxes at corresponding points of successive 2″ lattice cells, and could be analysed in the normal manner.

Lattice III. Measurements were again split into two interleaved 2″ interval sets. The 'even' set, A, was then of the same type as a Lattice I 2″ interval set. Set B was then composed of two interleaved 4″ interval sets, B1 and B2, corresponding respectively to the peaks and troughs of the fine–structure flux variation in successive lattice cells for which correction was made before analysis.

Lattice IV. In this case, the stack comprised too few lattice cells to allow splitting into "corresponding point" sets of data. The data were therefore analysed to yield a fine–structure function (found to be about 10% peak to trough amplitude) which was used to correct the data to a single set for cosine fitting. The error in the resulting points was increased to allow for uncertainties in the fine–structure function correction factors.

The least–squares fitted values of the extrapolated X–widths for each stack are given in Table 1. Good agreement is obtained in all cases for the extrapolated width at the two different levels of the stack, confirming freedom from higher harmonics in the X–direction.

4.4.2 N–S Widths (Y–widths)

Since a reasonably large bulk of moderator was always present between the counter and the nearest fuel strip, only relatively weak fine–structure variations were observed in y–width scans. For Lattices I and II, the symmetry was such that no corrections were required, while for Lattices III and IV, breaking into interleaved 2″ interval sets of data, reduced the remaining fine–structure 'ripples' to negligible proportions (total amplitude ~ 1 per cent.). This was covered by an increase in the errors assigned to the flux measurements for these runs.

The least–squares fitted values of the extrapolated Y–widths for each stack are given in Table 2. Whilst agreement between the widths measured at 12″ and 18″ levels was good for stacks III and IV, the discrepancies for stacks I and II suggested strongly the presence of a higher harmonic component in the y–direction flux distribution. This conclusion was supported by disagreement observed between relaxation lengths measured in the centre and the corner hole positions, before harmonic corrections were applied. Since the fitted widths displayed no significant asymmetry, the major higher harmonic contribution was assumed to be the third, and the 12″ level data were therefore re–analysed by least–squares fitting to the function:

$$\phi = A \cos \frac{\pi(y-\bar{y})}{a_y} + B \cos \frac{3\pi(y-\bar{y})}{a_y} \quad ,$$

where a_y is the extrapolated y-width,

$\bar{y}$ is the 'centre' of the distribution,

ϕ is the flux,

and A and B are amplitude coefficients.

The revised values (12" level) of a_y for Lattices I and II are given in Table 3, and are in excellent agreement with the 18" level measurements for which the harmonic content is negligible. The coefficients (B) of the third harmonic component derived from the 12" level measurements enabled the calculation of correction factors to reduce the observed vertical flux distributions for these lattices to the fundamental mode contribution only.

4.4.3 Relaxation Lengths

The vertical flux distributions for each lattice were least squares fitted to the function:

$$\phi = A \sinh \frac{h-z}{b_{11}} ,$$

where ϕ is the flux,

A is an amplitude coefficient,

h is the extrapolated height of the stack,

and b_{11} is the relaxation length of the fundamental mode.

Thus the relaxation lengths and extrapolated heights shown in Table 4 were derived. For Lattices I and II, the centre-hole flux values used in this analysis had been previously corrected to the fundamental mode using the harmonic coefficients derived in Section 4.4.2. It was arbitrarily decided to reject measurements for which the harmonic correction exceeded about 2 per cent. Corrections to the corner-hole fluxes were less than 0.05 per cent. and were therefore neglected.

4.4.4 Cadmium Ratio Measurements

Boron cadmium-ratio traverses were made along x, y, and z directions of each stack, and confirmed that within the experimental accuracy (approx. ±2 per cent.), the ratio was in all cases constant over the measuring range included in the analysis of the experiments.

4.4.5 Stack Dimensions

The overall dimensions of each stack were measured for each layer of tiles, and the mean values are given in Table 5. The quoted errors are due to irregularities in the building and clamping of the stacks.

4.4.6 Extrapolation Lengths

The extrapolation length λ_x or λ_y for each horizontal flux scan is given in Tables 1, 2, and 3. The extrapolated heights λ_h, from the vertical flux scans, are given in Table 4. The errors quoted do not include those due to uncertainties in the physical dimensions of the stacks (Table 5).

Table 6 gives the mean values of λ_x, λ_y, λ_h for each lattice. Although there is some suggestion that λ_x and λ_y may be increasing slightly as the spectrum softens, within the errors of the measurements, the trend is not significant, and the individual values are compatible with the overall mean values $\bar{\lambda}_x$, $\bar{\lambda}_y$, and $\bar{\lambda}_h$ given in Table 6.

When allowance for the uncertainties in the stack dimensions is made, $\bar{\lambda}_x$, $\bar{\lambda}_y$, and $\bar{\lambda}_h$ are consistent and give an overall mean extrapolation length:

$$\lambda = 1.77 \pm 0.1 \text{ cm},$$

which is in agreement with the value found in diffusion length measurements using these BeO tiles (Brittliff et al. 1963).

4.4.7 The Materials Buckling

The buckling components calculated from the measured values of extrapolated widths and relaxation lengths for each lattice are given in Table 7. The 'fitting' errors on the mean extrapolated widths have been increased to ± 0.3 cm where no fine-structure or harmonic effects are involved, and to ± 0.5 cm for the remainder, to allow for possible residual systematic effects (for example departure from true cosine distributions approaching the stack boundaries) whose presence may be indicated by the rather larger scatter of individual measured widths than would be expected from the statistical fitting errors. As a further consequence, width errors will be treated as non-independent in deriving the errors of the materials buckling.

Owing to the heterogeneous nature of the stacks, and the considerably longer transport mean free path in aluminium than in BeO, the migration area $M_{\parallel}^2$ in directions (x and z) parallel to the aluminium fuel location plates is expected to be greater than that, $M_{\perp}^2$, for the perpendicular (y) direction.

Under these conditions:

$$K^2 = \frac{M_{\parallel}^2}{M^2}\left\{\left(\frac{\pi}{a_x}\right)^2 - \left(\frac{1}{b_{11}}\right)^2\right\} + \frac{M_{\perp}^2}{M^2}\left(\frac{\pi}{a_y}\right)^2 ,$$

where

K^2 is the materials buckling of an homogeneous lattice of the same composition as the experimental stack (neglecting the effects of fine-structure flux depressions),

M^2 is the migration area in the corresponding homogeneous lattice,

and $M_{\parallel}^2$, $M_{\perp}^2$ are the migration areas for the experimental lattice, respectively parallel and perpendicular to the slabs.

No satisfactory method for the calculation of $\left(M_{\parallel}/M\right)^2$ or $\left(M_{\perp}/M\right)^2$ in slab geometry has been published and two-orientation method measurements of $M_{\parallel}^2/M_{\perp}^2$ would not be sufficiently accurate to be justifiable in the present lattices where the asymmetry can confidently be expected to be small. However, in the case (as in the present experiments) where the gaps are small compared with λ_s for the solid moderator, and the 'cell' width (2.74 cm) is small compared with the migration length (~ 12 cm for the most heavily absorbing lattice), Keane (1963 unpublished) has suggested a simple method for estimating $M_{\parallel}/M_{\perp}^2$, and we may assume without significant error that $M_{\perp}^2 \equiv M^2$.

Assuming the aluminium/fuel region to be replaced by vacuum, Keane's method gives $M_{\parallel}^2/M_{\perp}^2 = 1.034$ for Lattices I and II, and 1.017 for Lattices III and IV. When some attempt is made to allow for the presence of fuel and aluminium in the gap by uniform smearing, these figures are reduced to ~ 1.02 and 1.01 respectively.

Even if the higher asymmetry figures calculated above for vacuum in the fuel region are assumed to apply to the fuelled lattices, in no case does the correction to the materials buckling as calculated directly from the measured components exceed 0.4 of the experimental standard deviation. In practice, the required corrections are likely to be even smaller than this and no corrections for asymmetry have been included in the experimental materials buckling values given in Table 5. Corrections for neutron flux fine-structure must be calculated and applied to homogeneous system calculations before comparing them with these experimental data. The uncertainties in such corrections are expected to be larger than those due to neglecting the migration area asymmetry.

5. INTEGRAL SPECTRUM MEASUREMENTS

Measurements of the relative fission rates of U235, U233, and Pu239 in the lattices provide useful information regarding the adequacy of neutron-energy spectrum calculations both in the near-thermal and the epithermal energy ranges. The method used in the present measurements follows closely that of Campbell et al. (1958), and compares the relative reaction rates of ¼" diameter by 1" active length U235, U233, and Pu239 coated fission chambers in the lattice spectrum, and in a thermal column spectrum. The overall gain of the counting system was checked and fixed throughout the course of the measurements by use of a mercury pulser giving pulses of highly stable amplitude.

5.1 Lattice Measurements

The position of the active length of each fission chamber was determined by measurement of its X-radiograph. The chamber was then firmly attached to a 2-feet long aluminium extension tube on which was machined a mark exactly 35 cm from the centre of the active volume of the chamber. A polythene collar was then firmly fixed at the mark, thus ensuring that the depth of insertion of the counters in the vertical hole of the lattice was accurately reproducible. Accurate radial positioning was assured by the close fit of the aluminium extension tube in the vertical holes.

Two vertical holes were used in each lattice, position A being immediately adjacent to a fuel strip, and position B being as remote from the fuel as possible (Figure 8). Each lattice relative reaction rate measurement was "sandwiched" between two thermal column measurements.

5.2 Thermal Column Measurements

A convenient source of well-thermalised neutron flux is provided by the water shield-tank at the West end of the MOATA reactor (Marks 1962). At regions of sufficiently high flux, however, the gradients in this tank are very severe, and it was necessary to provide a "flattened" flux region by fixing an air-filled aluminium box 12" x 12" x 6" a few inches in front of the aluminium "window" which divides the graphite reflector from the shield tank. Access to the centre of the box was then obtained via an aluminium extension tube passing through, and fixed to it. This tube protruded well above the water level of the tank, and was closed at its lower end. By this means the flux gradients at the measuring depth were reduced to approximately ½ per cent. per cm along the tube and approximately 2 per cent. total variation from contact with the "back" wall of the tube to contact with the "front" wall for a ¼" diameter fission chamber.

For "thermal calibrations", the chambers were located by use of a long aluminium tube, which was attached by means of a grub screw to the 2-feet extension tube described in the last section. Radial location within the access tube was achieved by a small slip-on polythene collar which could be located a few inches above the fission chamber. The depth of insertion was fixed by a collar held by grub screw to the extension tube, and resting on the open end of the access tube.

5.3 Errors

The sources of random error contributing to the error of the measured lattice and thermal column fission-chamber count-rates are listed below. The magnitude of each is given as its contribution to the measured count-rate. In addition to these random errors, it is necessary to take account also of a number of possible sources of systematic error when assessing the absolute accuracy of the final fission ratios in the lattice spectra.

5.3.1 Random Errors - Thermal Calibration

(a) Statistical error

Approximately 100,000 counts were taken with each chamber, giving an error contribution of ~ 0.35 per cent.

(b) Reactor power and counter sensitivity drift

Counting was carried out against a mains controlled timing unit, or against a pre-set number of counts from a BF_3 proportional counter in the reactor shield tank. In either case, the error due to

drifts in reactor power or relative sensitivity of BF_3 counter compared with the fission chamber is approximately ± 0.35 per cent.

(c) Counter positioning

Uncertainty in the radial position of the chamber within the access tube contributed an error of approximately ± 0.5 per cent. to the count ratio. The axial positioning was accurate to better than ± 2 mm, contributing < ± 0.1 per cent. to the ratio.

(d) Overall gain of counting equipment

Drifts were observed in the gain of the equipment equivalent to approximately ± 2 volts in discriminator bias setting. Two sets of fission chambers were used during this series of measurements. For Set 1, this drift corresponded to < ± ½ per cent. error in the count ratios, and for Set 2, the corresponding error was in the range ± 1 to ± 1.4 per cent.

(e) Counter dead-time

For these small fission counters, the dead-time is much smaller than the paralysis time of the A.A.E.C. type 2A scaler fast decade input unit (2.5 ± 0.5 μs). The maximum dead-time correction was 2 per cent. so the resulting error did not exceed ± 0.4 per cent. of the count ratio.

Combination of the above independent sources of error gives the random error of a single thermal calibration ratio in the range of 0.9 – 1.6 per cent. Fifteen sets of measurements were made for the first set of chambers, and ten for the second set.

5.3.2 Random Errors – Lattice Measurements

The same sources of error were considered as discussed above in Section 5.3.1. The principal differences were that the statistical error and the positioning error were now each of the order of ±0.6 per cent., and the dead-time corrections were negligible.

5.3.3 Systematic Errors

In deriving the relative fission rate per fissile atom in the lattice spectrum from the fission chamber data, a number of effects giving rise to systematic errors must also be considered.

(a) Neutron absorption in the chamber walls

The wall absorption for each chamber will, in general, be different in the thermal column than in the lattice spectrum. This effect is normally corrected for by experimentally determining the wall depression by addition of successive sleeves of the wall material round the active length of the chamber. Unfortunately, in the present experiments this was not possible, as the wall-material, (NILO K), was unobtainable in Australia on the required time scale. However, measurements at A.E.E., Winfrith, with similar fission chambers having stainless-steel walls (Symons 1962 unpublished) showed that neglect of wall corrections in rather harder spectra than those of the present lattices could give systematic errors in the Pu^{239}/U^{235} fission ratio of up to 1½ per cent. Since Symons' data did not include U^{233}, and NILO K has somewhat different scattering/absorption properties to stainless steel, the error due to neglect of wall corrections has been taken as ± 2 per cent.

(b) Position of Active Volume

There is an uncertainty of approximately ± 1 mm in the positions of the centres of the active lengths of the chambers. Since the thermal calibrations are carried out in an effectively uniform flux whilst the gradient in the lattices was of the order of 5 per cent. per cm, this uncertainty contributes possible systematic errors to the fission ratios per fissile atom of 0.7 to 1 per cent.

(c) Fission Cross Section Data

To obtain the fission ratios per fissile atom, it is necessary to use published Maxwellian-averaged fission cross sections in conjunction with the thermal column measurements. These data were taken from Westcott (1961) and the relative accuracy is approximately ± 1 per cent.

5.3.4 Total Error

When all the foregoing sources of error are taken into account, the error in the fission ratio per fissile atom for any lattice is approximately ± 2½ per cent. The error in the fission ratio at position A relative to that for the same atoms at position B in any lattice is ± 1 per cent.

5.4 Results

The relative fission rates of the chambers used are given in Appendix VI for each lattice and for the thermal column. These values are normalised to the fission rate for the U235 chamber of each set.

The principal derived results are summarised in Table 8.

6. COMPARISON OF EXPERIMENTS WITH THEORY

Detailed calculations are in progress using multigroup transport and diffusion theory codes, and taking account by a number of models of the actual lattice geometries used. This work has been slowed by difficulty of access to an adequately large computer, and in order to avoid further delays in publication of the experimental data, the detailed experimental/theoretical comparison will be reported separately at a later date. Therefore as an interim measure only, simple spectrum calculations have been carried out for each lattice assuming a Maxwellian component of temperature:

$$T_n = T_p \left(1 + 1.84 \frac{\Sigma_a}{\xi \Sigma_s}\right) ,$$

(Coveyou et al. 1956) plus a '1/E' epithermal tail of strength

$$r = \frac{\Sigma_a}{\xi \Sigma_s}$$ (Westcott, 1961).

These parameters were used with the 'g' and 's' values of Westcott to derive the effective fission cross sections of U235, U233, and Pu239 in the experimental lattices. The calculated ratios for both the Δ_2 and Δ_4 forms of Westcott's joining function are compared with the experimental fission ratios in Table 9. The degree of agreement of each form with experiment is similar, except for the Pu239/U235 fission ratio in the harder spectra of lattices I and II where the Δ_2 form is markedly superior.

In order to calculate k_∞ for each composition, the above Δ_2 spectrum parameters were used to calculate the neutron utilisation of the fuel over the complete energy range, and the effective value of η. The (n,2n) enhancement was taken as 1.058 for all lattices, following Pollard (1963 unpublished). A U238 resonance escape probability was calculated in the usual way.

The Fermi Age was assumed to be that for the smeared moderator, neglecting the presence of other materials, based on $\tau = 110$ cm^2 for $\rho = 2.8$ g/cm^3. The diffusion area, L^2, was taken as that for smeared-density BeO times the ratio of BeO absorption to total absorption in the lattice. The calculated materials buckling was then given by

$$k_\infty = (1 + L^2 B_M^2)\, e^{B_M^2 \tau} .$$

These values are compared with the measured bucklings in Table 9.

7. CONCLUSIONS

The materials bucklings of the four chosen BeO/U235 lattices have been measured to an accuracy of approximately ± 4 per cent. Relative fission ratios have been measured to approximately ± 3 per cent. To within ± 1 per cent, no differences were observed between the fission ratios measured in contact with a fuel strip, and in a position in the lattice cell as remote from the fuel as possible.

Simple calculations have been made of the fission ratios and materials bucklings of homogeneous systems of the same composition as the experimental lattices. The agreement with the experimental results is surprisingly satisfactory in view of the limited applicability of the calculations to the conditions of the experiments, and the neglect of any allowance for fine-structure flux depressions. It is of interest to note that Westcott's Δ_2 cut-off model gives substantially better agreement with the plutonium reaction rate in the harder spectra of Lattices I and II than does the Δ_4 model. It is however dangerous to conclude that this is the better model to use for prediction of temperature effects in BeO moderated lattices, since the elevation of neutron temperature and the r-values appropriate to Lattices I and II exceeded by substantial amounts the limits given by Westcott for the range of validity of these spectrum assumptions. It is considered unprofitable therefore, despite the measure of agreement with the present experiments, to pursue these methods of calculation further, since little if any confidence could be placed in their predictions of temperature and long term reactivity effects, particularly for systems incorporating significant quantities of resonance absorbers.

A comparison of the experimental data with the results of refined calculations will be made at a later date in a separate report.

8. ACKNOWLEDGMENTS

Miss E. Kletzmayr's assistance in all aspects of data processing on the IBM 1620 computer is gratefully acknowledged. Thanks are due also to Mr. J. Griffiths and the MOATA operations team for counting and general assistance in the experimental work.

9. REFERENCES

Brittliff, E., Duerden, P., and McCulloch, D.B. (1963). – AAEC/TM203.

Campbell, C.G., Freemantle, R.G., and Poole, M.J. (1958). – AERE R/R 2398.

Coveyou, R.R., Bate, R.R., and Osborn, R.K. (1956). – J. Nucl. Energy 2: 153.

Finke, R.G. (1962). – UCRL 6980.

Kloverstrom, F.A., Deck, R.M.R. and Reyenga, A.J. (1959). – UCRL 5369, Pt. I.

Kloverstrom, F.A. and Kraft, D.E. (1960). – UCRL 5369, Pt. II.

Kloverstrom, F.A., Deck, R.M.R., and Reyenga, A.J. (1960). – Nucl. Sci. and Engng. 8, No. 3, Sept. 1960.

Marks, A.P. (1962). – Atomic Energy, 5 (4): 9-21. Australian Atomic Energy Commission.

Morton, J.R., Shon, F.J., Weirich, T.F., Gardner, L.L. (1962). – UCRL 6729.

TABLE 1

EXTRAPOLATED X–WIDTHS

Lattice	12″ level						18″ level					
	Set	No. of Points	a_x (cm)	$\bar{x}$ (cm)	$\Sigma \frac{\delta^2}{\sigma^2}$	λ_x (cm)	Set	No. of Points	a_x (cm)	$\bar{x}$ (cm)	$\Sigma \frac{\delta^2}{\sigma^2}$	λ_x (cm)
I	A	6	49.68 ±0.30	22.94 ±0.14	15.9	1.90 ±0.15	A	6	48.87 ±0.37	22.99 ±0.17	1.7	1.50 ±0.19
	B	5	48.68 ±0.51	22.61 ±0.23	1.3	1.40 ±0.15	B	5	49.33 ±0.64	22.67 ±0.28	1.0	1.73 ±0.32
II		11	49.61 ±0.38	22.81 ±0.18	5.5	1.87 ±0.19		11	49.83 ±0.38	22.76 ±0.18	15.0	1.98 ±0.19
III	A	8	65.16 ±0.31	30.53 ±0.14	6.3	1.98 ±0.16	A	8	65.19 ±0.31	30.71 ±0.14	8.1	1.99 ±0.16
	B	8	64.98 ±0.42	30.46 ±0.21	4.2	1.89 ±0.21	B	8	64.32 ±0.41	30.54 ±0.20	1.1	1.56 ±0.21
IV		14	65.13 ±0.64	30.42 ±0.20	20.5	1.96 ±0.32		14	65.56 ±0.65	30.58 ±0.20	18.0	2.17 ±0.32

TABLE 2

EXTRAPOLATED Y–WIDTHS

Lattice	12″ level						18″ level					
	Set	No. of Points	a_y (cm)	$\bar{y}$ (cm)	$\Sigma \frac{\delta^2}{\sigma^2}$	λ_y (cm)	Set	No. of Points	a_y (cm)	$\bar{y}$ (cm)	$\Sigma \frac{\delta^2}{\sigma^2}$	λ_y (cm)
I	A	9	52.28 ±0.40	23.13 ±0.27	3.5	2.80 ±0.20	A	9	49.95 ±0.52	23.29 ±0.35	0.9	1.64 ±0.26
	B	9	52.47 ±0.38	23.03 ±0.26	17.8	2.90 ±0.19	B	9	49.17 ±0.49	23.41 ±0.34	8.2	1.25 ±0.25
II		9	51.25 ±0.44	23.23 ±0.31	6.0	2.29 ±0.22		9	49.35 ±0.57	23.46 ±0.40	1.1	1.34 ±0.29
III	A	9	66.56 ±0.27	31.78 ±0.20	10.0	1.49 ±0.14	A	9	66.76 ±0.27	32.05 ±0.20	2.1	1.59 ±0.14
	B	8	66.94 ±0.43	31.80 ±0.30	3.1	1.68 ±0.22	B	8	67.13 ±0.43	32.09 ±0.30	6.4	1.78 ±0.22
IV	A	9	66.94 ±0.28	31.71 ±0.20	5.9	1.68 ±0.14	A	9	67.04 ±0.28	31.83 ±0.20	4.6	1.73 ±0.14
	B	8	66.54 ±0.42	31.73 ±0.30	8.6	1.48 ±0.21	B	8	66.64 ±0.40	31.94 ±0.29	1.3	1.53 ±0.20

TABLE 3

LATTICES I AND II (12″ LEVEL) Y–WIDTHS WITH THIRD HARMONIC COMPONENT

Lattice	Set	No. of Points	A_1	A_3	a_y (cm)	y (cm)	$\Sigma \frac{\delta^2}{\sigma^2}$	λ_y
I	A	9	8966	– 17.1	49.40 ±0.5	23.24 ±0.35	2.9	1.36 ±0.25
	B	9	9744	– 16.4	49.89 ±0.5	23.02 ±0.35	17.2	1.61 ±0.25
II		9	19480	– 246	49.44 ±0.6	23.24 ±0.4	5.6	1.38 ±0.3

TABLE 4

RELAXATION LENGTHS AND EXTRAPOLATED HEIGHTS

Lattice	Centre Hole				Corner Holes							
					North East				South West			
	b_{11} (cm)	h (cm)	No. of Points	$\Sigma \frac{\delta^2}{\sigma^2}$	b_{11} (cm)	h (cm)	No. of Points	$\Sigma \frac{\delta^2}{\sigma^2}$	b_{11} (cm)	h (cm)	No. of Points	$\Sigma \frac{\delta^2}{\sigma^2}$
I	19.40 ±0.70	63.85 ±1.14	6	3.2	19.68 ±0.56	63.65 ±1.10	6	6.9	20.13 ±0.61	63.52 ±1.08	6	7.6
II	16.70 ±0.40	63.03 ±0.95	10	9.4	16.82 ±0.32	62.27 ±0.75	11	5.2	16.70 ±0.31	63.69 ±0.94	11	25.9
III	28.70 ±1.8	63.17 ±0.66	9	8.3	28.25 ±1.9	62.74 ±0.65	9	5.4				
IV	20.95 ±0.46	63.16 ±0.60	11	7.7	21.35 ±0.52	62.19 ±0.53	11	5.7				

TABLE 5

MEASURED STACK DIMENSIONS

Lattice	E–W (X) (cm)	N–S (Y) (cm)	Height (cm)
I AND II	45.88 ± 0.10	46.68 ± 0.15	61.05 ± 0.05
III AND IV	61.21 ± 0.10	63.58 ± 0.15	61.05 ± 0.05

TABLE 6

MEAN VALUES OF EXTRAPOLATION LENGTHS

Lattice	λ_x (cm)	λ_y (cm)	λ_h (cm)
I	1.69 ± 0.10	1.47 ± 0.13	2.57 ± 0.63
II	1.92 ± 0.13	1.36 ± 0.21	1.77 ± 0.50
III	1.89 ± 0.09	1.60 ± 0.09	2.35 ± 0.46
IV	2.06 ± 0.23	1.64 ± 0.09	1.53 ± 0.41
Overall Means	$\bar{\lambda}_x$ = 1.84 ± 0.12	$\bar{\lambda}_y$ = 1.58 ± 0.16	$\bar{\lambda}_h$ = 1.96 ± 0.27

TABLE 7

THE MATERIALS BUCKLING

Lattice	$(\pi/a_x)^2$ (m^{-2})	$(\pi/a_y)^2$ (m^{-2})	$(1/b_{11})^2$ (m^{-2})	K^2 (m^{-2})
I	40.65 ± 0.50	40.11 ± 0.79	25.90 ± 1.3	54.9 ± 1.8
II	39.93 ± 0.48	40.82 ± 0.81	35.73 ± 0.90	45.0 ± 1.6
III	23.31 ± 0.36	22.13 ± 0.33	12.29 ± 0.69	33.2 ± 1.0
IV	23.11 ± 0.34	22.08 ± 0.33	22.36 ± 0.74	22.8 ± 1.0

TABLE 8

THE MEASURED FISSION RATIOS

Lattice	POSITION A		POSITION B		A relative to B	
	Pu239/U235	U233/U235	Pu239/U235	U233/U235	Pu239/U235	U233/U235
I	2.12 ± 0.05	1.26 ± 0.03	2.13 ± 0.05	1.26 ± 0.03	0.994 ± 0.009	1.000 ± 0.009
II	1.86 ± 0.05	1.11 ± 0.03	1.86 ± 0.05	1.10 ± 0.03	1.000 ± 0.009	1.003 ± 0.009
III	1.66 ± 0.04	1.03 ± 0.03	1.68 ± 0.04	1.03 ± 0.03	0.991 ± 0.009	0.993 ± 0.009
IV	1.57 ± 0.04	1.03 ± 0.03	1.56 ± 0.04	1.03 ± 0.03	1.004 ± 0.009	0.996 ± 0.009

TABLE 9

COMPARISON OF EXPERIMENTAL RESULTS WITH SIMPLE CALCULATIONS

Lattice	FISSION RATIOS				MATERIALS BUCKLING	
	239/235		233/235		Experiment (m^{-2})	Calculation (m^{-2})
	Experiment	Calculation	Experiment	Calculation		
		Δ_2 Δ_4		Δ_2 and Δ_4		
I	2.12 ± 0.05	2.27 2.53	1.26 ± 0.03	1.35	54.9 ± 1.8	50
II	1.86 ± 0.05	1.85 1.98	1.10 ± 0.03	1.14	45.0 ± 1.6	42
III	1.67 ± 0.04	1.62 1.68	1.03 ± 0.03	1.03	33.2 ± 1.0	37
IV	1.56 ± 0.04	1.54 1.59	1.03 ± 0.03	1.00	22.8 ± 1.0	29

APPENDIX I

LATTICE I FLUX MEASUREMENTS

(a) Widths (E–W)

	12″ level		18″ level	
x (cm)	ϕ	σ	ϕ	σ
9.91*	8159	41	2522	17
12.45	9636	48	3001	20
14.99*	10680	53	3316	22
17.53	11580	58	3550	24
20.07*	12000	60	3717	25
22.61	12140	61	3778	25
25.15*	11860	59	3729	25
27.69	11520	58	3578	24
30.23*	10730	54	3379	23
32.77	9659	48	3012	20
35.31*	8631	43	2670	18

NOTE * and plain values form two interleaved sets of data.

(b) Widths (N–S)

	12″ level (A)		18″ level (A)		12″ level (B)		18″ level (B)	
y (cm)	ϕ	σ	ϕ	σ	ϕ	σ	ϕ	σ
12.09	6892	35	3941	26	7621	38	4286	29
14.83	7738	39	4462	30	8518	43	4836	32
17.58	8297	42	4846	32	8975	45	5232	35
20.32	8627	43	5086	34	9376	47	5629	38
23.06	8783	44	5189	35	9603	48	5677	38
25.81	8746	44	5088	34	9533	48	5663	38
28.55	8389	42	4906	33	9146	46	5375	36
31.29	7796	39	4548	30	8448	42	4981	33
34.03	7015	35	4038	27	7544	38	4425	30

(continued)

APPENDIX I (continued)

(c) Relaxation Lengths

z (cm)	Centre Hole			Corner Hole (NE)		Corner Hole (SW)	
	ϕ	Harmonic Correction (Add)	σ	ϕ	σ	ϕ	σ
22.95	–	–	–	17390	167	17410	173
28.03	15319	325	130	13170	126	13020	143
33.11	11816	128	107	10090	112	9970	116
38.19	8697	50	84	7690	94	7740	94
43.27	6447	20	52	5400	55	5540	55
48.35	4485	8	40	3850	43	3860	43

APPENDIX II

LATTICE II FLUX MEASUREMENTS

(a) Widths (E–W)

	12″ level		18″ level	
x (cm)	ϕ	σ	ϕ	σ
9.91	18180	136	5097	38
12.45	20720	155	5906	44
14.99	23000	173	6553	49
17.53	24760	186	6895	52
20.07	25840	194	7258	54
22.61	26370	198	7428	56
25.15	26210	197	7310	55
27.69	25240	190	6992	52
30.23	23470	176	6640	50
32.77	21240	159	6073	46
35.31	18440	138	5131	39

(b) Widths (N–S)

	12″ level		18″ level	
y (cm)	ϕ	σ	ϕ	σ
12.45	15120	113	2357	18
15.19	17000	128	2643	20
17.93	18420	138	2869	22
20.68	19100	143	3013	23
23.42	19040	143	3045	23
26.16	19010	143	2979	22
28.90	17980	135	2843	21
31.65	16800	126	2601	20
34.39	14940	112	2307	17

(c) Relaxation Lengths

	Centre Hole			Corner Hole (NE)		Corner Hole (SW)	
z (cm)	ϕ	Harmonic Correction (Add)	σ	ϕ	σ	ϕ	σ
24.15	–	–	–	17760	173	17880	176
26.69	17290	349	195	15400	157	15110	147
29.23	14490	216	164	13050	137	12850	131
31.77	12660	134	138	11100	115	10670	114
34.31	10800	83	122	9536	109	9194	107
36.85	9326	51	106	8141	97	7989	92
39.39	7645	32	89	6906	82	6830	79
41.93	6422	20	74	5677	77	5883	74
44.47	5428	12	65	4711	61	4792	58
47.01	4520	7	56	3828	51	3866	49
49.55	3591	5	48	3139	41	3137	41

APPENDIX III

LATTICE III FLUX MEASUREMENTS

(a) Widths (E–W)

	12″ level		18″ level			12″ level *		18″ level *	
x (cm)	ϕ	σ	ϕ	σ	x (cm)	ϕ	σ	ϕ	σ
10.23	11160	56	5241	26	12.77	13180	92	6186	43
15.31	15020	75	7045	35	17.85	16840	115	7812	55
20.39	17760	89	8475	42	22.93	18940	133	8940	63
25.47	19480	97	9189	46	28.01	20050	140	9463	66
30.55	19900	100	9488	47	33.09	19780	139	9485	66
35.63	19480	97	9262	46	38.17	18670	131	8914	62
40.71	17690	88	8421	42	43.25	16500	116	7820	55
45.79	14880	74	7144	36	48.33	13060	92	6163	43

* Fine–structure corrected.

(b) Widths (N–S)

	12″ level		18″ level			12″ level		18″ level	
y (cm)	ϕ	σ	ϕ	σ	y (cm)	ϕ	σ	ϕ	σ
10.95	11710	82	4864	34	13.69	13910	97	5785	40
16.23	15660	110	6532	46	18.97	17530	123	7305	51
21.52	18780	131	7809	55	24.26	19720	138	8208	57
26.80	20600	144	8638	61	29.54	21120	148	8884	62
32.08	21330	149	8905	62	34.82	20980	147	8794	62
37.37	20380	143	8681	61	40.11	19470	136	8324	58
42.65	18450	129	7775	54	45.39	16890	118	7160	50
47.93	15040	105	6503	45	50.67	13410	94	5745	40
53.21	11330	79	4849	34					

(continued)

APPENDIX III (continued)

(c) Relaxation Lengths

	Centre Hole		Corner Hole	
z (cm)	ϕ	σ	ϕ	σ
29.23	13270	106	7974	74
31.77	12100	88	6996	68
34.31	10560	85	6279	55
36.85	9402	78	5585	52
39.39	8377	75	4866	47
41.93	7373	59	4336	43
44.47	6285	59	3684	33
47.01	5309	49	3124	28
49.55	4455	44	2562	25

APPENDIX IV

LATTICE IV FLUX MEASUREMENTS

(a) Widths (E–W)

	12″ level *		18″ level *	
x (cm)	ϕ	σ	ϕ	σ
12.77	11280	113	4782	48
15.31	12410	124	5353	54
17.85	13680	137	5838	58
20.39	14570	146	6217	62
22.93	15590	156	6656	67
25.47	16270	163	6913	69
28.01	16900	169	7204	72
30.55	16950	169	7231	72
33.09	16920	169	7277	73
35.63	16380	164	7024	70
38.17	15530	155	6695	67
40.71	14570	146	6286	63
43.25	13660	137	5891	59
45.79	12400	124	5353	54

* After correction for fine–structure.

(b) Widths (N–S)

	12″ level		18″ level			12″ level		18″ level	
y (cm)	ϕ	σ	ϕ	σ	y (cm)	ϕ	σ	ϕ	σ
10.95	9702	68	3601	25	13.69	11410	80	4218	30
16.23	13130	92	4748	33	18.97	14380	101	5330	37
21.52	15360	108	5647	40	24.26	16160	113	6043	42
26.80	16980	119	6308	44	29.54	17370	122	6452	45
32.08	17360	122	6419	45	34.82	17190	120	6405	45
37.37	16690	117	6217	44	40.11	15810	111	5989	42
42.65	15020	105	5601	39	45.39	14030	98	5238	37
47.93	12650	89	4677	33	50.67	10830	76	4110	29
53.21	9245	65	3457	24					

(continued)

APPENDIX IV (continued)

(c) Relaxation Lengths

	Centre Hole		Corner Hole	
z (cm)	ϕ	σ	ϕ	σ
24.15	17270	137	9073	82
26.69	14990	116	7896	70
29.23	13120	108	7094	68
31.77	11520	101	6097	57
34.31	10110	90	5349	52
36.85	8873	80	4624	45
39.39	7644	73	4053	39
41.93	6513	62	3420	35
44.47	5470	50	2912	29
47.01	4686	46	2436	25
49.55	3776	38	1955	20

APPENDIX V

LATTICE MATERIALS

(a) Composition of Homogeneously Smeared Experimental Lattices in Atoms per cm^3

Material	Lattice			
	I	II	III	IV
BeO	6.378×10^{22}	6.378×10^{22}	6.641×10^{22}	6.641×10^{22}
Al	3.885×10^{21}	3.191×10^{21}	1.662×10^{21}	1.541×10^{21}
U235	4.353×10^{19}	2.177×10^{19}	1.133×10^{19}	7.555×10^{18}
U238	3.072×10^{18}	1.536×10^{18}	7.996×10^{17}	5.332×10^{17}
U236	1.597×10^{18}	7.986×10^{17}	4.156×10^{17}	2.772×10^{17}
U234	4.868×10^{17}	2.435×10^{17}	1.267×10^{17}	8.450×10^{16}

(b) Mean Fuel Strip Data

Dimensions: 24.0" x 1.330" x 0.040"

Composition: Aluminium 53.11 g

Uranium 16.24 g

Isotopic Composition of Uranium (atom per cent.).

U234	U235	U236	U238
1.00	89.41	3.28	6.31

(c) Aluminium Lattice Plates

Material: 99.95 per cent. Pure Aluminium.

Dimensions: (i) 24" x 18" x 0.080" – weight 860 g.

or

(ii) 24" x 6" x 0.080" – weight 287 g.

APPENDIX VI

RELATIVE FISSION RATES IN THE LATTICES

Counter Type	Lattice I		Lattice II		Lattice III		Lattice IV		Thermal Column	Relative Effective Number of Fissile Atoms in Chamber
	POS. A	POS. B	POS. A	POS. B	POS. A	POS. B	POS. A	POS. B		
U235	1.000 ±0.006	1.000 ±0.006	1.000 ±0.007	1.000 ±0.007	–	–	–	–	1.0000 ±0.0017	1.000 ±0.0017
U233	0.368 ±0.003	0.368 ±0.003	0.324 ±0.003	0.323 ±0.003	–	–	–	–	0.2731 ±0.0007	0.2928 ±0.0007
Pu239	0.626 ±0.006	0.630 ±0.006	0.549 ±0.005	0.549 ±0.005	–	–	–	–	0.4086 ±0.0010	0.2956 ±0.0007
U235	–	–	–	–	1.000 ±0.006	1.000 ±0.006	1.000 ±0.006	1.000 ±0.006	1.0000 ±0.0023	1.0000 ±0.0023
U233	–	–	–	–	0.296 ±0.004	0.298 ±0.004	0.295 ±0.005	0.296 ±0.005	0.2686 ±0.0014	0.3251 ±0.0017
Pu239	–	–	–	–	0.540 ±0.007	0.545 ±0.007	0.509 ±0.007	0.507 ±0.007	0.4494 ±0.0018	0.2880 ±0.0012

NOTES (i) Relative effective numbers of fissile atoms for each chamber were calculated using effective 20.44 °C Maxwellian average cross sections given by Westcott (1961) σ_{f5} = 563.1b, σ_{f3} = 525.2b, σ_{f9} = 778.3b.

(ii) The Pu239 chamber was common to both sets.

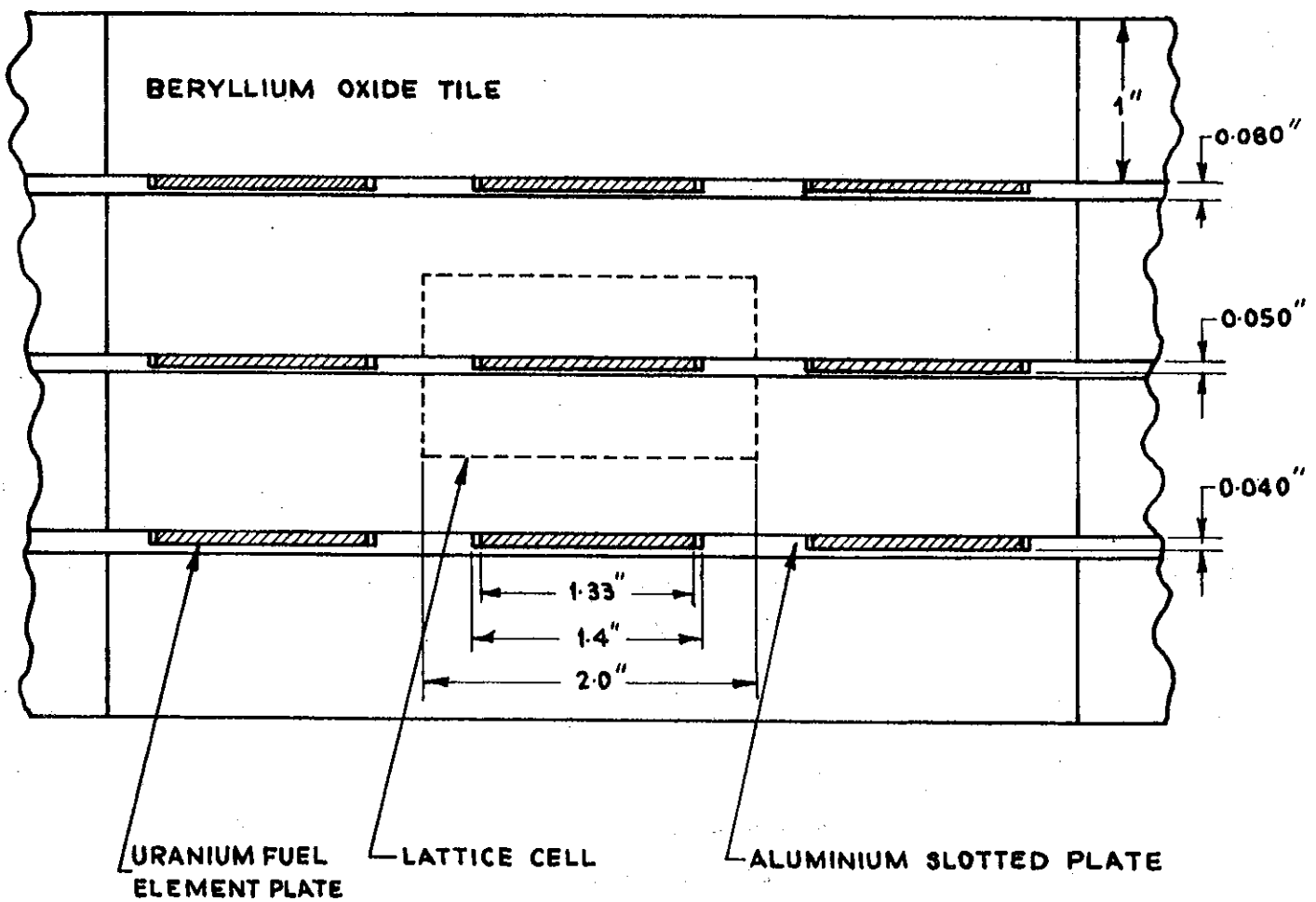

FIGURE 1 – LATTICE I – REPRESENTATIVE SECTION OF TOP FACE

P626

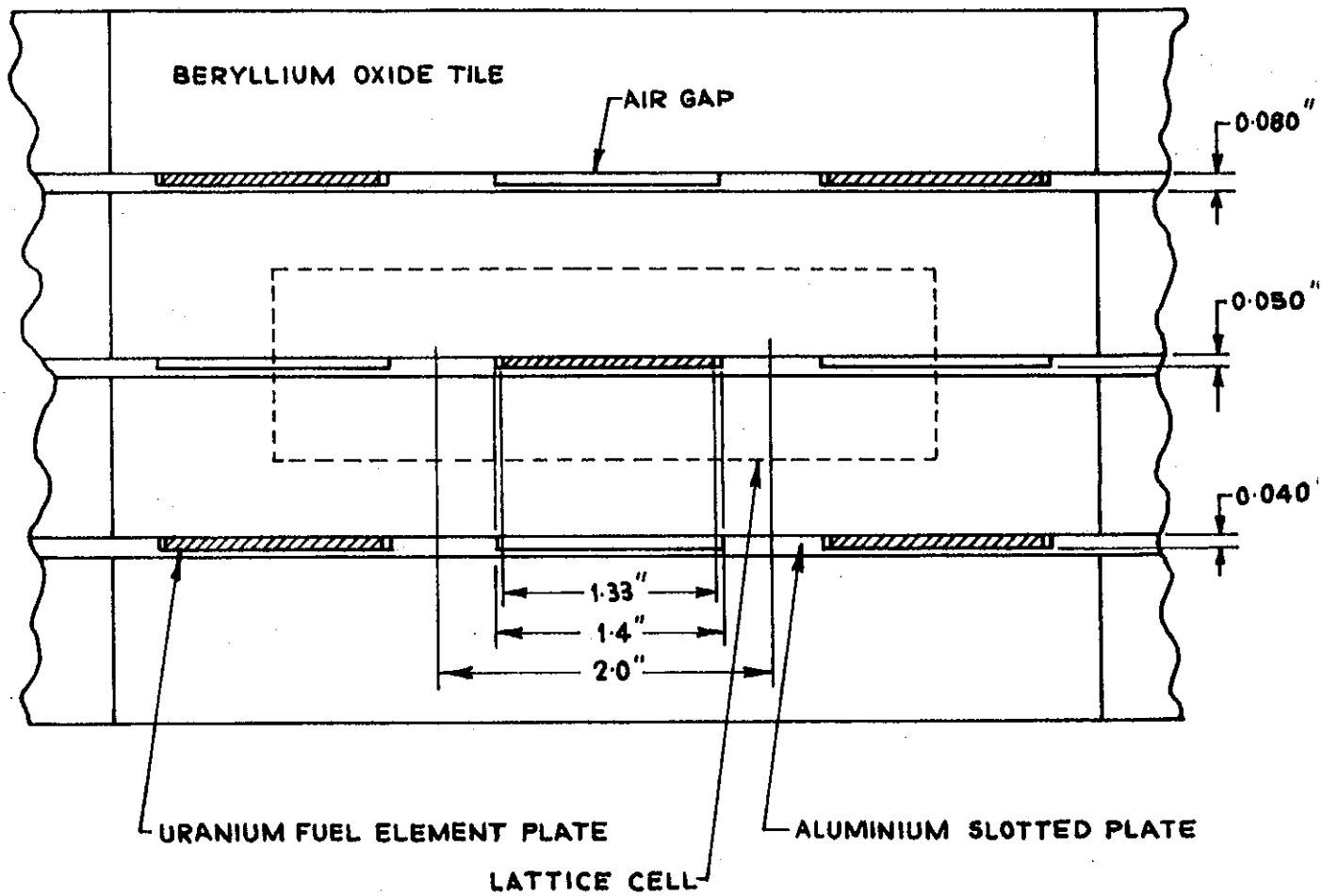

FIGURE 2. LATTICE II – REPRESENTATIVE SECTION OF TOP FACE

P626

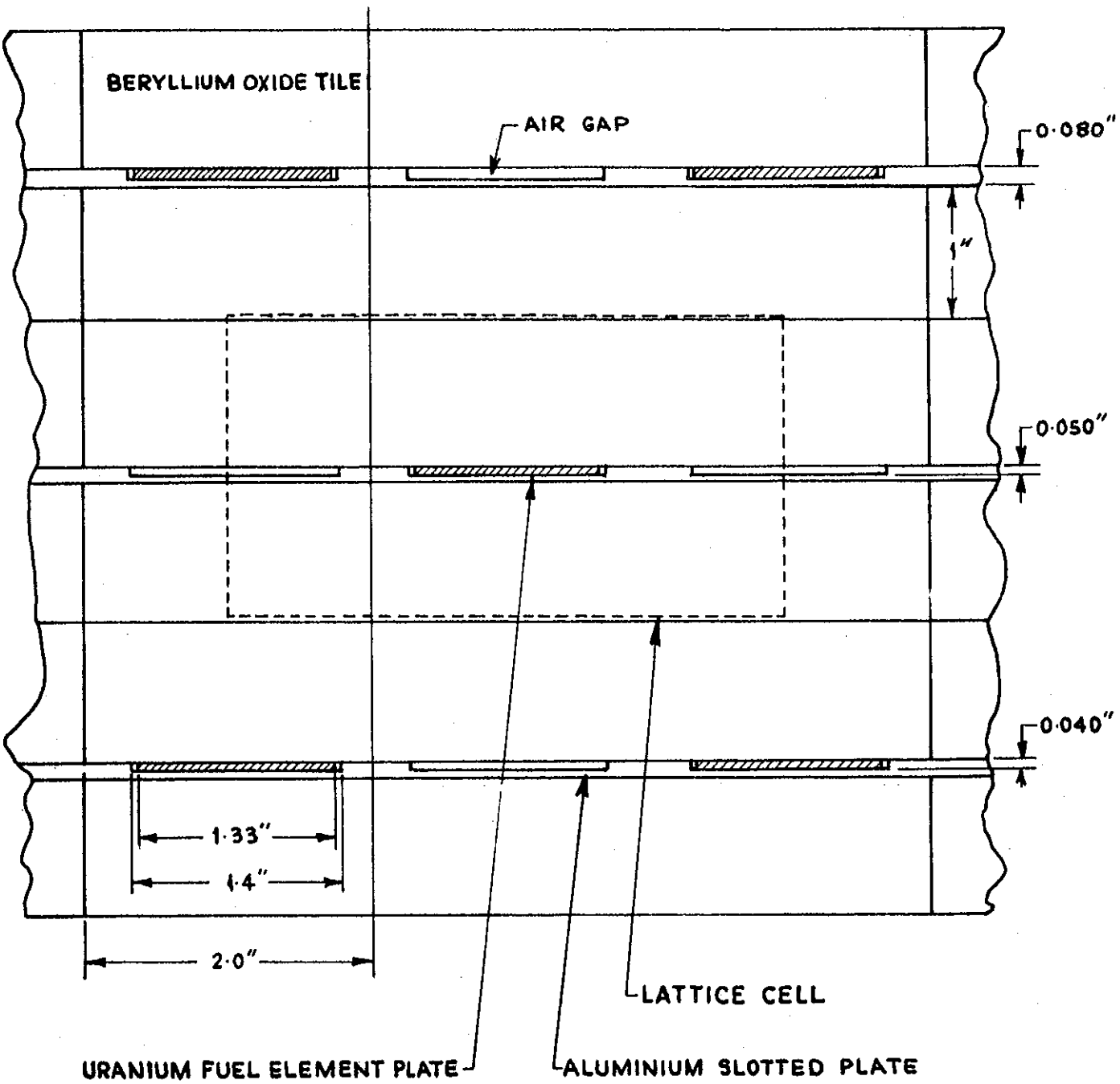

FIGURE 3. LATTICE III – REPRESENTATIVE SECTION OF TOP FACE

P626

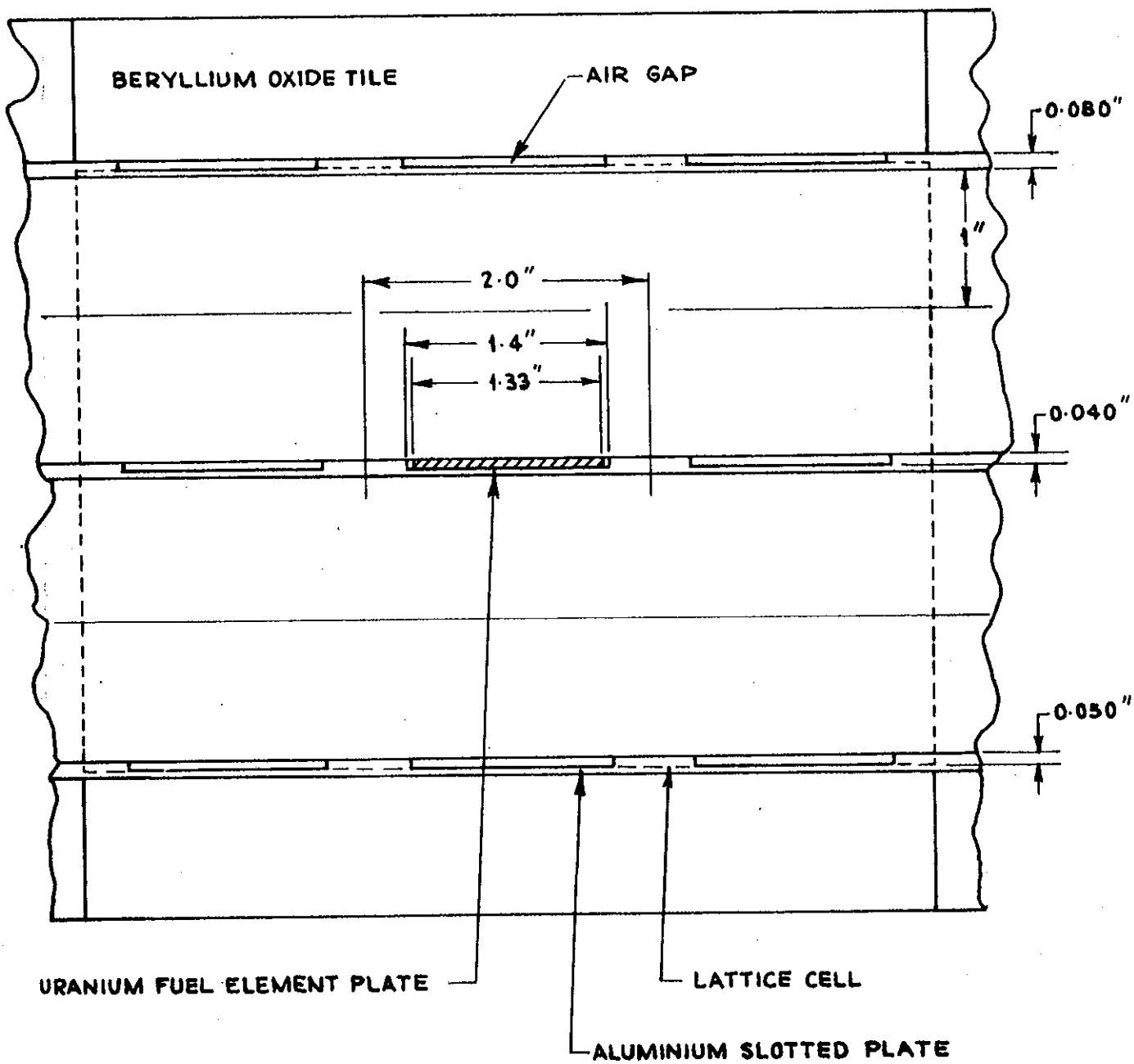

FIGURE 4. LATTICE IV – REPRESENTATIVE SECTION OF TOP FACE

P626

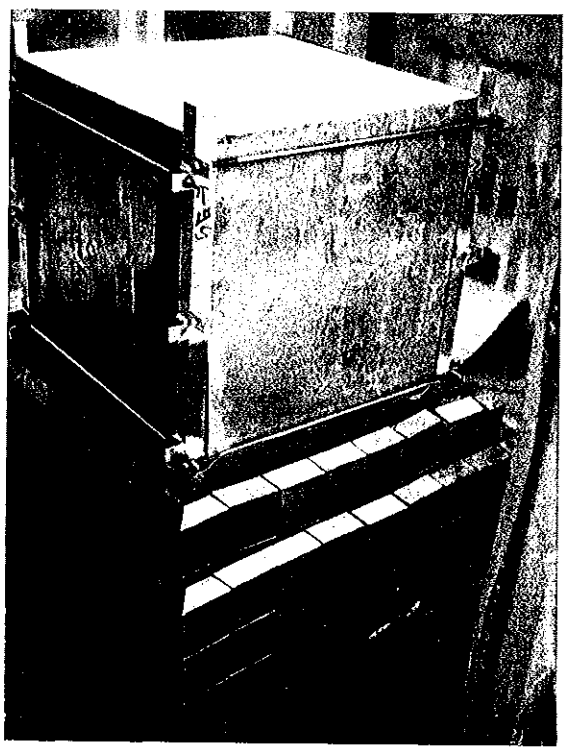

FIGURE 5 GENERAL VIEW OF STACK FOR LATTICE I

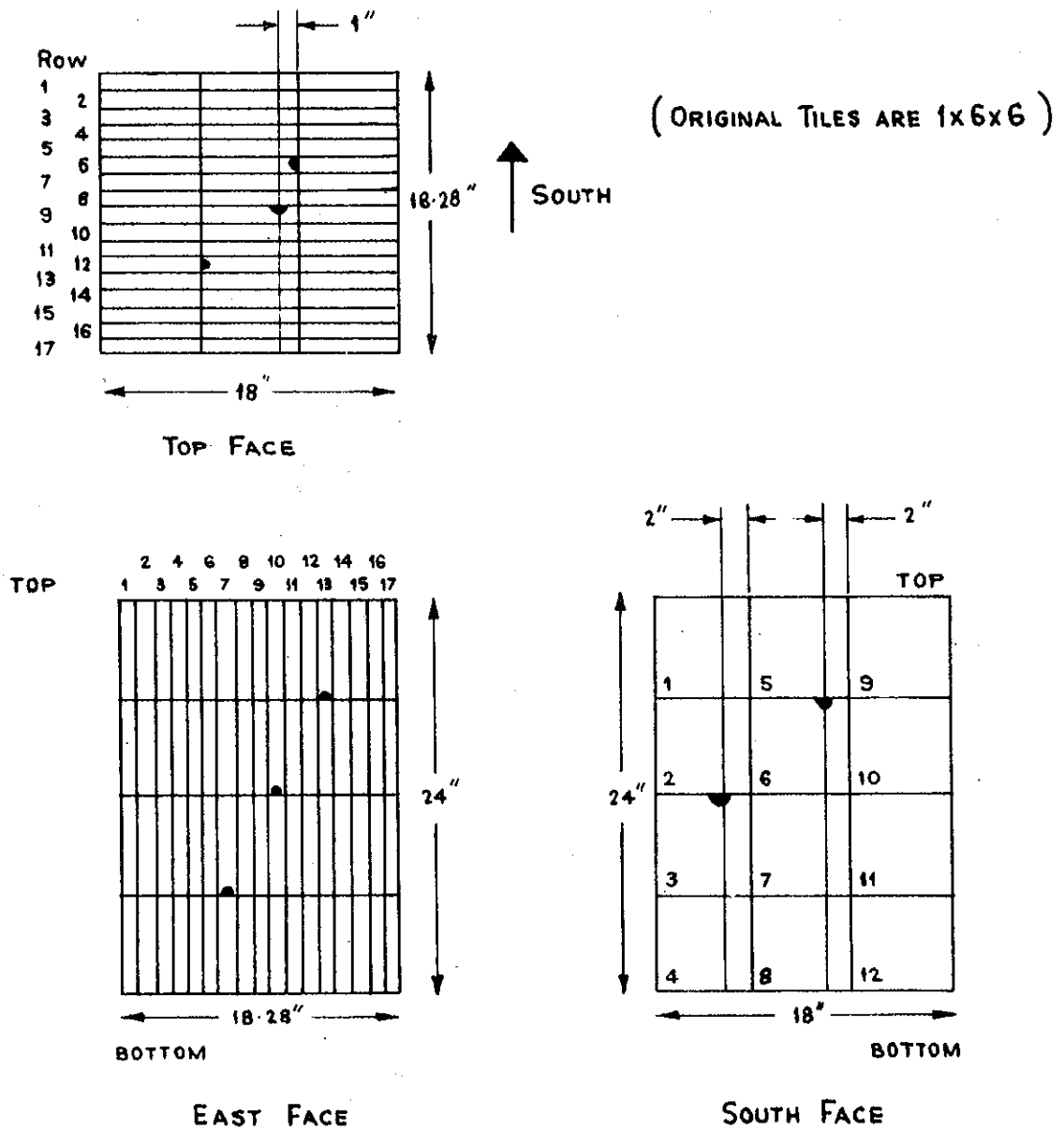

FIGURE 6. SCANNING HOLE POSITIONS IN SMALL STACK (LATTICES I & II)

P626

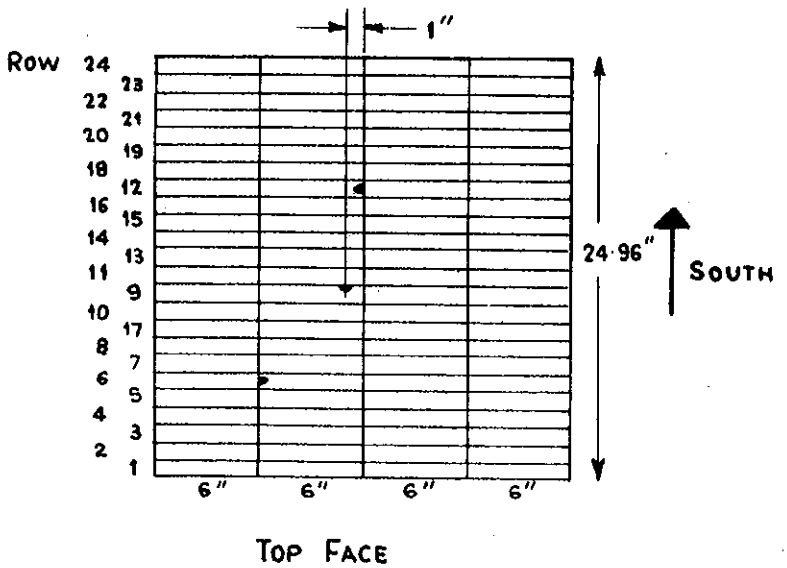

Top Face

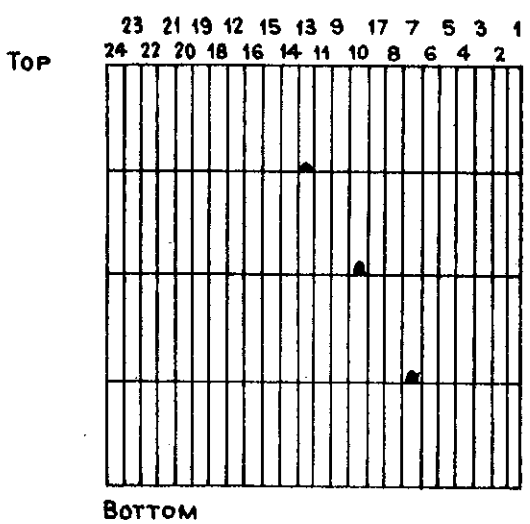

East Face

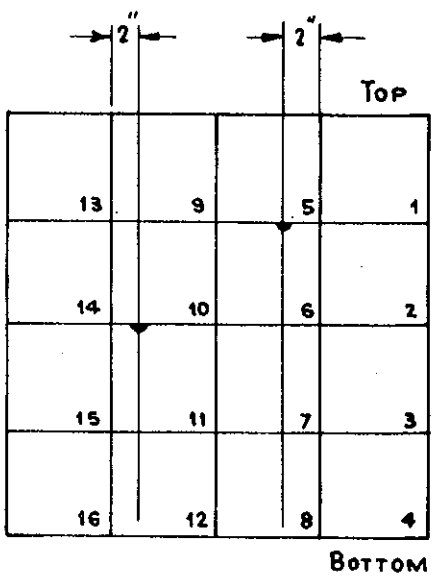

South Face

Figure 7. Scanning Hole Positions in Large Stack (Lattices III & IV)

P626

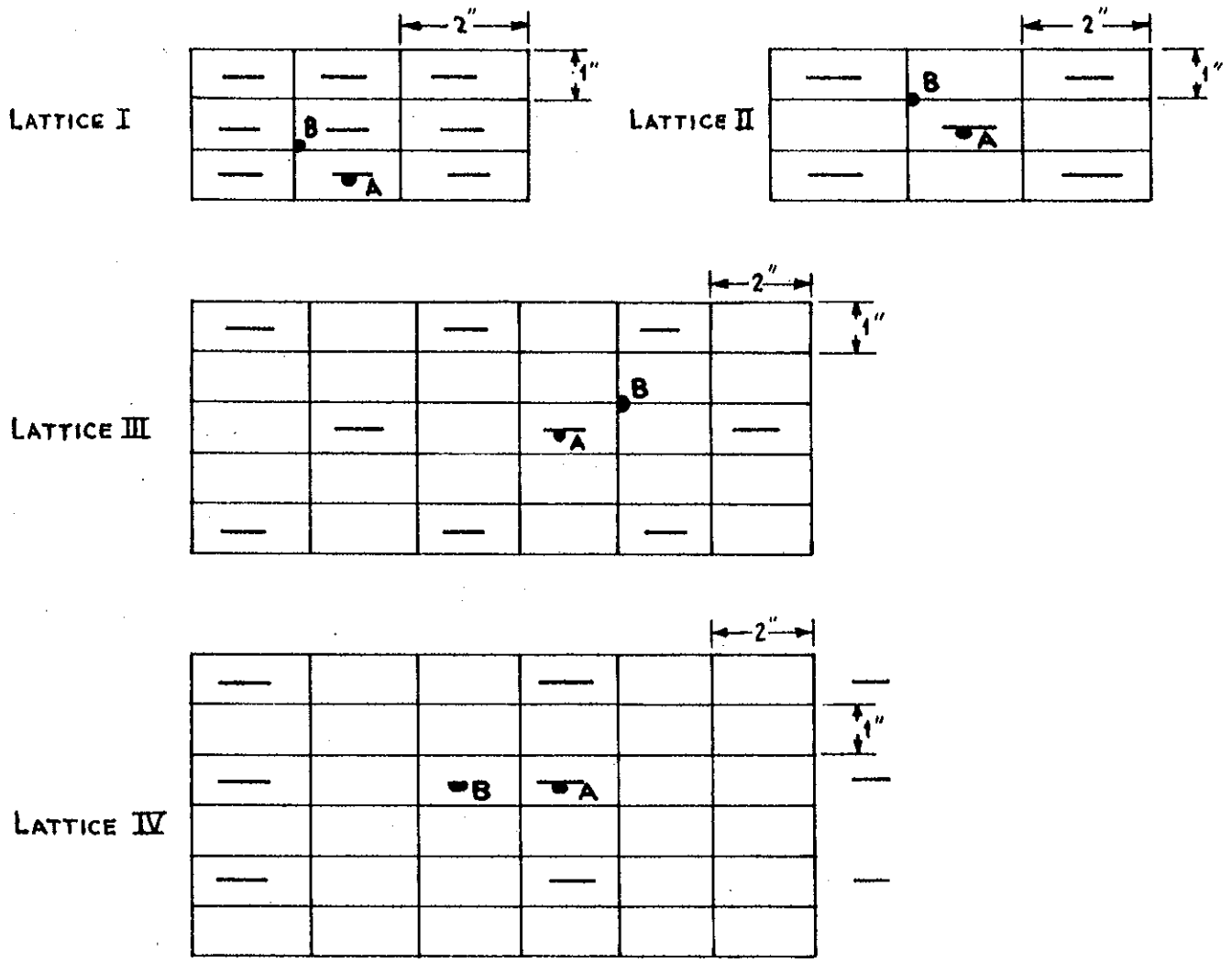

FIGURE 8. RELATIVE POSITIONS OF HOLES FOR INTEGRAL SPECTRUM MEASUREMENT
Note: These diagrams show only the positions of A & B holes relative to the fuel. They do not give their positions relative to each other, nor their absolute positions in the lattice.

P626